Appl. Phys. B 85, 427–435 (2006)
DOI: 10.1007/s00340-006-2301-3

**Applied Physics B**
**Lasers and Optics**

K. NAMJOU[1]
C.B. ROLLER[1,✉]
T.E. REICH[1]
J.D. JEFFERS[1]
G.L. MCMILLEN[1]
P.J. MCCANN[2]
M.A. CAMP[3]

# Determination of exhaled nitric oxide distributions in a diverse sample population using tunable diode laser absorption spectroscopy

[1] Ekips Technologies, Inc., Norman, OK 73069, USA
[2] School of Electrical and Computer Engineering, University of Oklahoma, Norman, OK 73019, USA
[3] The Lung Center, Inc., Norman, OK 73071, USA

**Received: 30 March 2006/Revised version: 3 May 2006**
**Published online: 23 June 2006 • © Springer-Verlag 2006**

**ABSTRACT** A liquid-nitrogen free mid-infrared tunable diode laser absorption spectroscopy (TDLAS) system equipped with a folded-optical-path astigmatic Herriott cell was used to measure levels of exhaled nitric oxide (eNO) and exhaled carbon dioxide ($eCO_2$) in breath. Quantification of absolute eNO concentrations was performed using $NO/CO_2$ absorption ratios measured by the TDLAS system coupled with absolute $eCO_2$ concentrations measured with a non-dispersive infrared sensor. This technique eliminated the need for routine calibrations using standard cylinder gases. The TDLAS system was used to measure eNO in children and adults ($n = 799$, ages 5 to 64) over a period of more than one year as part of a field study. Volunteers for the study self-reported data including age, height, weight, and health status. The resulting data were used to assess system performance and to generate eNO and $eCO_2$ distributions, which were found to be log-normal and Gaussian, respectively. There were statistically significant differences in mean eNO levels for males and females as well as for healthy and steroid naïve asthmatic volunteers not taking corticosteroid therapies. Ambient NO levels affected measured eNO concentrations only slightly, but this effect was not statistically significant.

**PACS** 33.20.Ea; 42.62.Be; 82.80.Gk; 87.80.-g

## 1 Introduction

Recent clinical research has established a firm link between high levels of exhaled nitric oxide (eNO) and airway inflammation [1]. This link is significant for a number of reasons. First, it provides a noninvasive clinical test to assess lower airway inflammation, a chronic condition in asthmatic patients. Second, eNO measurements can be used to monitor the effectiveness of anti-inflammatory therapies (i.e., inhaled corticosteroids), as well as treatment compliance as it is well established that eNO values fall when people with asthma are properly treated [2]. The United States Food and Drug Administration (USFDA) approved measurement of eNO for monitoring anti-inflammatory therapy prescribed for asthma in 2003. Spirometric tests measure only mechanical aspects of airway health rather than a chemical biomarker associated with the underlying disease, airway inflammation.

✉ Fax: 405-307-8807, E-mail: cbroller@ekipstech.com

Chemiluminescence is presently the most widely used technique to measure eNO in children and adults. This method detects NO by its reaction with ozone to produce $NO_2$ and light, where the light is measured with a photomultiplier tube. As with most laboratory analytical techniques, commercially available chemiluminescence instruments require frequent calibration. Calibration is accomplished using a standard gas sample having a known NO concentration (typically $200 \pm 20$ ppb), and is recommended every two weeks, when the instrument is moved, after re-powering and following significant ambient temperature changes. Emerging technologies, including electrochemical sensors (for example Aerocrine's Mino®) and chemically reactive substrates (Aperon Biosystems' Sol Gel technology), offer the promise of inexpensive eNO breath measurements. These technologies, however, are not capable of real-time detection and can require more than one minute to obtain results. It remains unclear if such technologies will be capable of adequate breath collection standardization in terms of regulating exhalation flow rates, eliminating affects of ambient NO, and discarding NO originating from the nasal cavity across large populations in order to achieve clinically useful results.

Laser spectroscopic techniques for breath analysis have been used to measure a number of clinically relevant biomarkers including exhaled ammonia to monitor renal dialysis [3], exhaled ethane for assessing oxidative stress and exposure [4, 5], and eNO for evaluating lower airway inflammation [6–9]. There are a number of additional biomarkers in expired breath suitable for laser spectroscopy and include formaldehyde, acetaldehyde, carbonyl sulfide, and carbon disulfide as indicators for breast cancer [10], lung cancer [11], organ rejection [12], and schizophrenia [13], respectively. The work reported here focuses on the development of a tunable diode laser absorption spectroscopy (TDLAS) sensor for routine measurement of eNO. TDLAS in the mid-infrared region ($\sim 5.2\,\mu$m) of the electromagnetic spectrum where strong fundamental absorption bands for NO reside is particularly well suited for eNO measurement because NO and $CO_2$ can be measured during the same laser scan (effectively simultaneously). The advantages of this technique are discussed below.

In previous publications, we have described the development of a TDLAS technique that can be used to measure NO and $CO_2$ simultaneously in exhaled breath [6, 7]. It was shown

that the patient's own $CO_2$ could serve as an internal calibrant gas for the TDLAS sensor, thus eliminating frequent calibrations with standard cylinder gases and removing potential systematic errors. Visual inspection of the measured exhaled $CO_2$ trend with the TDLAS sensor can be used to confirm proper breath sample collection. In addition, $CO_2$ levels measured simultaneously with NO can alert the instrument operator to potential anomalies in the operation of the TDLAS sensor. The importance of this point cannot be overstated. Aldeen and coworkers examined side-by-side comparisons of two commercially available chemiluminescence instruments over a 3.5-month period on an individual with no known lung disease [14]. On two occasions, they noted significant measurement deviations of eNO levels from baseline values up to 150% due to issues with the instrumentation. These deviations occurred with no identifiable problems with the subject and repeated calibrations did not resolve the measurement errors. They concluded that biologic controls (i.e., measurement of an individual with a known baseline eNO level) could be used to detect problems due to a lack of measurable metrics internal to the chemiluminescence sensors.

TDLAS, to date, has not been widely utilized as a tool for breath analysis, and issues regarding performance in the field and in a clinical setting remain unknown. This paper describes the use of a liquid-nitrogen-free TDLAS system, termed the Breathmeter$^{TM}$, for measurement of eNO in children and adults as part of a large clinical field study. Analytical methods used to calibrate the TDLAS sensor internally using measured $NO/CO_2$ absorption ratios coupled with absolute concentrations of exhaled $CO_2$ measured with a NDIR-$CO_2$ sensor are covered. The results of a study in which using the TDLAS sensor successfully measured eNO from 769 volunteers are given along with a discussion of sensor performance in terms of accuracy and precision. Additionally, a brief discussion of future development plans for reducing the size and cost of the TDLAS sensor are provided.

## 2 Experimental setup and procedures

### 2.1 *System overview*

In this study, eNO breath analysis is based on high-resolution absorption spectroscopy using a single-mode mid-infrared diode laser operating near 5.2 μm. The experimental setup is shown in Fig. 1. The cold head within the cryostat housing contains a IV-VI (Pb-salt) semiconductor tunable diode laser source, an infrared HgCdTe photovoltaic detector, a foil heater, and a temperature sensor. The present system employs a closed-cycle refrigerator system (Helix IGC Polycold, Petaluma, CA) that continuously cools the diode laser and detector to cryogenic temperatures ($> 80$ K) with no need for liquid nitrogen. An auto-tuning temperature controller (LakeShore, Westerville, OH) is used to maintain laser temperatures at set points between 85 and 110 K with an accuracy of 0.01 K.

The output laser beam is collimated with a $f/1$ off-axis-parabolic mirror and focused with a plano-concave mirror (Janos, Townshend, VT) into the pressure controlled Herriott cell (Aerodyne, Billerica, MA) with a 36 m optical path length and a 0.3-liter volume. Upon exiting the cell, the transmitted beam is then collected and focused onto the infrared detector by an $f/1.5$ aspheric lens. Absorption spectra are obtained by sweeping the laser wavelength over absorption features of NO and $CO_2$ using a 100-Hz sawtooth tuning waveform (specific NO and $CO_2$ spectral regions measured are discussed in greater detail below). An ac modulation current ($\sim 42$ kHz triangle waveform) is superimposed onto the 100 Hz sweep signal to modulate the laser emission wavelength for the purpose of harmonic detection. Both waveforms are generated using standard function generators (Stanford Research Systems, Sunnyvale, CA) and fed into the laser current controller (Newport, Irvine, CA). The photo-detector signal is pre-amplified (Fermionics, Simi Valley, CA) prior to being sampled at twice the modulation frequency by a DSP lock-in amplifier (Stanford Research Systems, Sunnyvale, CA). The 2nd harmonic ($2f$) absorption signal from the output of the lock-in amplifier is sampled using a data acquisition card (National Instruments, Austin, TX) with 12-bits of resolution. The digital TTL trigger signal from the sawtooth ramp function generator is used to start each acquisition and acquire 500-points per laser scan. The computer stores individual laser scans and performs a running coverage of 75 sequential scans to improve signal-to-noise ratios. Control of all electronics, signal acquisition, and data analysis is provided through a LabView-based graphical user interface software program using RS-232 communications, GPIB, and a PCI bus.

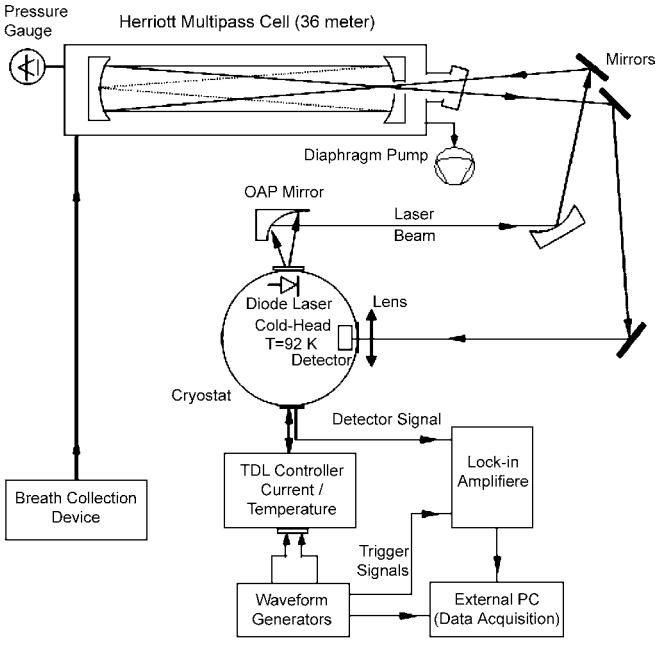


**FIGURE 1** System schematic of the TDLAS sensor designed to measure eNO and $eCO_2$. Major components include a cryostat, Herriott multipass cell, electronics, and an integrated breath collection apparatus

Slight thermal variations of the laser can cause wavelength drift of the absorption spectra in respect to the injection current. In lieu of an acquired reference arm signal using a second gas cell and detector, an $H_2O$ absorption line with an unambiguous peak is used to align the acquired spectra in memory prior to averaging. For large spectral drifts, the laser wavelength is corrected by adjusting the laser current.

An oil-free diaphragm pump (Vaccuubrand, Essex, CT) and an integrated gas flow controller ($\pm 0.05$ L min$^{-1}$ accuracy, Alicat Scientific, Tucson, AZ) were used to maintain

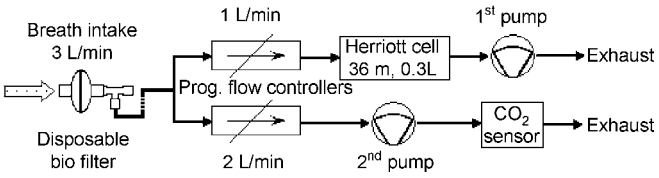


**FIGURE 2** Schematic diagram of the breath collection apparatus consisting of a biologic mouthpiece, custom T-piece equipped with two one-way flutter valves, mass flow controllers, and two flow paths. A NDIR-$CO_2$ sensor is placed in one path to quantify exhaled $CO_2$ concentrations

a gas cell pressure of 5.85 kPa (45 Torr) and a constant flow of 1.0 standard liters per minute (slpm, at standard temperature and pressure of 296 K and 1 atm). A pressure transducer (MKS Instrument, Andover, MA) was used to measure the pressure inside the gas cell. Teflon tubing was used for all connections in the gas sampling system. For collection of breath to measure eNO, the American Thoracic Society (ATS) recommends a constant exhalation flow rate of 3 slpm at an exhalation pressure of 5 to 20 cm $H_2O$ or 0.5 to 2 kPa [15]. In order to meet this requirement, a second path is provided via an additional flow controller set at 2 slpm and a second smaller pump to induce flow, see Fig. 2. Along the second path, absolute exhaled $CO_2$ concentrations are measured using an inline NDIR-$CO_2$ sensor (Conspec Control, Charleroi, PA).

### 2.2 *Spectral region*

Candidate NO and $CO_2$ absorption features for the analysis of exhaled breath samples were identified with the aid of spectral line positions in the HITRAN database [16], such that NO and $CO_2$ absorptions features were sufficiently close in proximity to be measured using a single laser scan and without interference from each other or other molecular species. According to the HITRAN database, fundamental absorption lines for NO are located between 1820 $cm^{-1}$ and 1920 $cm^{-1}$ ($\sim 5.2\,\mu m$). Four candidate line pairs have been identified for NO and $CO_2$, and they are in the vicinity of 1900.5 $cm^{-1}$, 1912.1 $cm^{-1}$, 1912.8 $cm^{-1}$, and 1915.0 $cm^{-1}$. Each identified spectral region contained a strong NO line(s) ($> 10^{-20}$ cm molecule$^{-1}$ line strength), at least one weak $CO_2$ line (around $10^{-25}$ cm molecule$^{-1}$), and one strong $CO_2$ or $H_2O$ line ($> 10^{-23}$ cm molecule$^{-1}$) with an unambiguous absorption feature for spectral alignment purposes, where all lines are in the vicinity of each other ($< 0.2$ $cm^{-1}$) without overlapping. Here, we describe results obtained using the NO and $CO_2$ line pair at 1914.98 $cm^{-1}$ and 1915.54 $cm^{-1}$, respectively. Figure 3 shows measured second harmonic absorption spectra for a non-asthmatic breath sample in the 1915 $cm^{-1}$ region and the corresponding HITRAN line positions and intensities. The strong $H_2O$ line at 1915.19 $cm^{-1}$ was used for spectral centering in this example.

### 2.3 *Single breath collection and measurements*

In this study, the single breath on-line measurement method was used according to the recommendations of the ATS for measurement of eNO [15]. A disposable antibacterial mouthpiece is connected to one port of a custom designed T-piece (see Fig. 2). The three ports of the T-piece consist of two one-way flutter valves and a barbed adapter

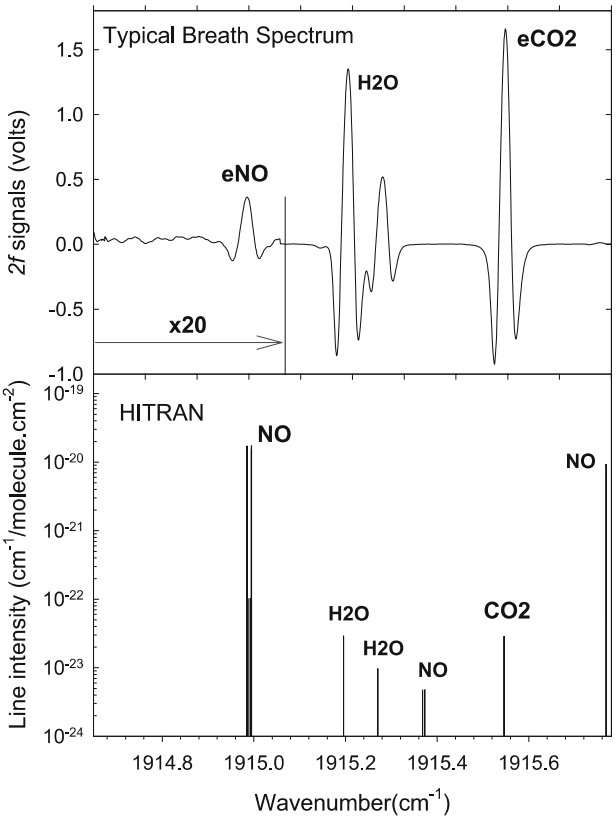


**FIGURE 3** (*Upper plot*) Laser absorption spectrum in the 1915 $cm^{-1}$ spectral range of an exhaled breath sample from a non-asthmatic volunteer where the eNO absorption feature is magnified by a factor of 20. The $H_2O$ absorption feature is used to align spectra and maintain laser wavelengths. (*Lower plot*) The corresponding HITRAN-96 lines were used to identify molecular absorption features

connected to 1/4″ Teflon tubing. The first flutter valve prevents inhalation through the mouthpiece and the second flutter valve opens in the event of negative pressure buildup, for example if a subject blocks the induced gas flow during exhalation. This is a safety feature designed to prevent the pump from sucking a subject's tongue or lip into the mouthpiece. Teflon tubing connects the T-piece to the breath collection apparatus.

Volunteers were instructed to exhale with a force greater than 5 cm $H_2O$ ($> 0.5$ kPa) for a period of not less than 10-s and not more then 15-s. The resulting resistance against exhalation and the associated back pressure in the upper airway was monitored by using integrated pressure transducers within the input port of the mass flow controllers. The exhalation pressure was displayed on the computer screen during testing in order to provide feedback to the patient and instrument operator. For each volunteer, three breath samples were collected and analyzed. Institutional Review Board approval for human subjects research was obtained through Western IRB (Olympia, WA), and each volunteer (or parent or guardian) signed a consent form prior to breath donation.

The upper two plots of Fig. 4 show absorption trends for eNO and $eCO_2$ over a single exhalation measured using the TDLAS sensor, and the lower plot shows the corresponding absolute $eCO_2$ concentration, as measured using the NDIR-$CO_2$ sensor. It should be noted that the absolute $CO_2$ concen-

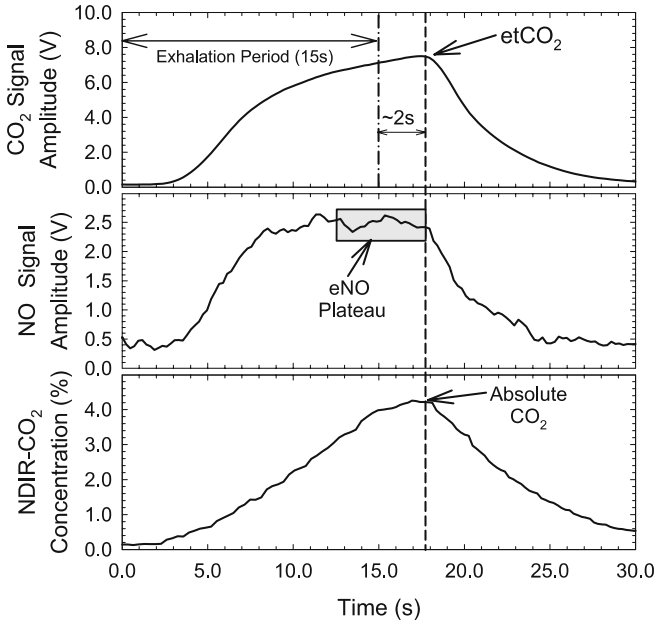


**FIGURE 4** (*Upper plot*) Exhaled $CO_2$ trend as measured by the TDLAS sensor showing the exhalation period of 15 s, sensor delay time of $\sim 2$ s, and the $etCO_2$ point. (*Middle plot*) Exhaled NO trend indicating the eNO plateau used to determine the eNO concentration. (*Lower plot*) Exhaled $CO_2$ trend as measured by the NDIR-$CO_2$ sensor

trations measured with the NDIR sensor are used to quantify the qualitative data captured using the TDLAS instrument. The $2f$ measurement technique cannot be used to quantify concentrations from first principles, which is possible when using direct absorption techniques. Future work is planned to investigate direct $CO_2$ concentration determination using custom electronics and analysis algorithms. The end-tidal $CO_2$ ($etCO_2$) in the $CO_2$ exhalation trend (upper plot) marks the point where the eNO plateau and absolute $CO_2$ concentration are to be determined. The eNO plateau is defined as all eNO points 4-s before the $etCO_2$ point. These points are averaged to determine the reported eNO concentration. Note that $etCO_2$ appears about 2 s after the end of the exhalation period. This is due to a delay associated with gas transit and data processing times. Determination of absolute eNO concentrations from the measured eNO and $etCO_2$ absorption magnitudes and the absolute $etCO_2$ concentration is described in the next section. It should be noted that this method does not require discard bags to eliminate upper airway breath from being measured as was necessary in prior TDLAS measurements of eNO [6, 7]. The fast gas exchange time associated with this smaller volume Herriott cell (0.3 l) as compared to the white cell (16 l) allows real-time measurement of the entire breath sample.

### 2.4 *Measurement of* $etCO_2$ *and* eNO *concentrations*

Simultaneous measurement of end-tidal $CO_2$ ($etCO_2$) and eNO in the same laser spectral sweep allows one to determine analytically the absolute eNO concentration using $eNO/etCO_2$ signal ratios, absorption constants in the HITRAN database, and absolute $CO_2$ concentrations measured using the NDIR-$CO_2$ sensor. Figure 4 provides graphical illustrations for the determination of the $etCO_2$ absorption magnitude (upper plot), eNO plateau (middle plot), and the absolute $etCO_2$ concentration (lower plot).

Beer's law for small absorption allows the concentration of one molecular species to be determined using another species of known concentration by taking the ratio between the two species. First, several assumptions have been made in this method:

1. NO concentration does not exceed 400-ppb and $etCO_2$ concentration does not exceed 6% such that the absorbances of the selected NO and $CO_2$ lines behave in a linear fashion,
2. the incident or non-absorbed laser intensity across the closely selected lines for NO and $CO_2$ (in a $\sim 0.2\,\mathrm{cm}^{-1}$ spectral range) is assumed to be equivalent,
3. the second harmonic signal amplitudes for NO and $CO_2$ correlate linearly with the magnitude of the direct absorption signal such that the transform function between the two schemes will be cancelled out when using the ratio method, and
4. the pressure in the spectrometer's gas cell is the same as when the proportionality constant for the $NO/CO_2$ ratio is determined using calibration gases.

According to Beer's law for small absorbances ($< 12\%$), the number of molecules-per-$cm^3$ or the number density ($n$) of a trace gas at certain pressure and temperature is given by:

$$n = \frac{A}{\sigma L} \tag{1}$$

where, $\sigma$ is the absorption cross section ($cm^2$/molecule), $L$ is the optical path length (cm) in the gas medium, and $A$ is the light absorbance. Since the ratio of the number density of two gases ($n_1$ and $n_2$) is equal to their concentration ($C$) ratio, the concentration ratio of two trace gases can be shown as:

$$\frac{C_1}{C_2} = \frac{\sigma_2}{\sigma_1}\frac{A_1}{A_2} \tag{2}$$

where,

$$\sigma_i = \sum_m S_m(\nu_{0i})\varphi_m(\nu_{0i}) \tag{3}$$

and

$$A_i = \frac{\Delta I_i}{I_{0i}}\,, \tag{4}$$

where $\nu_0$ is the center line frequency, and $i$ refers to the specific molecular species. $S(\nu_0)$ is the molecular line intensity which is given in the HITRAN database in units of ($\mathrm{cm}^{-1}$/molecule $\mathrm{cm}^{-2}$), $\varphi(\nu_0)$ is the magnitude of line shape function (Voigt profile) at the absorption center in units of (cm), $m$ refers to number of unresolved NO lines in the selected spectral region, in this study $m = 12$ for NO and $m = 1$ for $CO_2$. $\Delta I$ is the direct absorption peak intensity, and $I_{0i}$ is the incident laser intensity at selected wavelengths for NO ($i = 1$) and $CO_2$ ($i = 2$) lines. Based on the second assumption, the ratio of laser powers ($I_{02}/I_{01}$) is about one. The summation in (3) reflects the fact that NO absorption feature can incorporate multiple absorption lines over a $0.001\,\mathrm{cm}^{-1}$

range, which are not resolvable mainly due to the finite instrument resolution ($\sim 0.002\,\mathrm{cm}^{-1}$).

The ratio of eNO to et$CO_2$ peak intensity at the time of breath testing is compared with the ratio of these molecules when calibrated at known concentrations (references), which were previously measured at the same conditions in terms of temperature, pressure, and modulation amplitude. This method is introduced to cancel out all spectroscopic parameters and to improve the absorption cross section ratio as used in our previous works [6, 7]. During routine breath testing, the method only needs the absorption peak intensities, which is sufficient to calculate the eNO concentration. Using (1), the ratio of two gas mixtures of NO and $CO_2$, one with known concentrations (ref) in a gas mixture can be shown as:

$$\frac{C_{\mathrm{NO}}}{C_{\mathrm{CO_2}}} = \frac{\sigma_{\mathrm{CO_2}}}{\sigma_{\mathrm{NO}}} \frac{A_{\mathrm{NO}}}{A_{\mathrm{CO_2}}} \tag{5}$$

and

$$\frac{C_{\mathrm{refNO}}}{C_{\mathrm{refCO_2}}} = \frac{\sigma_{\mathrm{refCO_2}}}{\sigma_{\mathrm{refNO}}} \frac{A_{\mathrm{refNO}}}{A_{\mathrm{refCO_2}}} \,. \tag{6}$$

Then the ratio of (5) to (6) is:

$$\frac{C_{\mathrm{NO}} C_{\mathrm{refNO}}}{C_{\mathrm{CO_2}} C_{\mathrm{refCO_2}}} = \frac{\sigma_{\mathrm{CO_2}} \sigma_{\mathrm{refCO_2}}}{\sigma_{\mathrm{NO}} \sigma_{\mathrm{refNO}}} \frac{A_{\mathrm{NO}} A_{\mathrm{refNO}}}{A_{\mathrm{CO_2}} A_{\mathrm{refCO_2}}} \,. \tag{7}$$

Since $\sigma$ remains unchanged for each gas molecule, and considering (2)–(4) above, (7) can be simplified as:

$$C_{\mathrm{NO}} = \left[ \frac{V_{\mathrm{refCO_2}}}{V_{\mathrm{refNO}}} \frac{C_{\mathrm{refNO}}}{C_{\mathrm{refCO_2}}} \right] \frac{V_{\mathrm{NO}}}{V_{\mathrm{CO_2}}} C_{\mathrm{CO_2}} \,, \tag{8}$$

where $V_{\mathrm{NO}}$, $V_{\mathrm{CO_2}}$ and $V_{\mathrm{refNO}}$, $V_{\mathrm{refCO_2}}$ represent the measured $2f$ absorption signal magnitudes (in volts) for NO and $CO_2$ in the breath sample and the signal magnitudes in a reference gas of concentrations $C_{\mathrm{refNO}}$ and $C_{\mathrm{refCO_2}}$, respectively. The signal to concentration ratio can be related to the absorption cross section ($\sigma$) as:

$$\frac{V_{\mathrm{refCO_2}}/C_{\mathrm{refCO_2}}}{V_{\mathrm{refNO}}/C_{\mathrm{refNO}}} = \frac{\sigma_{\mathrm{refCO_2}}}{\sigma_{\mathrm{refNO}}} \,. \tag{9}$$

In fact, the numerator and denominator in the right-hand side of (9) represent the slopes of the linear calibration curves of $CO_2$ and NO, respectively. This ratio provides a constant number for a pair of selected NO and $CO_2$ molecular absorption lines at certain wavelengths stated in the previous section. At the same experimental conditions, such as gas partial pressure, temperature, and modulation amplitude, a variation in the optical power does not change the ratio number. Equation (9) can be rewritten as:

$$C_{\mathrm{NO}} = \left[ \frac{\text{slope of } \mathrm{CO_2} \text{ cal curve}}{\text{slope of NO cal curve}} \right] \frac{V_{\mathrm{NO}}}{V_{\mathrm{CO_2}}} C_{\mathrm{CO_2}} \,. \tag{10}$$

To calibrate the system using calibration curves, a mixture of different but known concentrations of $CO_2$ and NO (from zero to 5% $CO_2$ and from zero to 200 ppb NO) using a combination of two precise mass flow controllers is sent to a mixing chamber prior to the gas cell. During calibration, the TDLAS remains under the same system conditions as when breath testing. The procedure is repeated at least 10 times throughout the day; the average of the slopes of the calibration curves for each molecule is calculated and inserted in (10). In measuring the absorption cross sections ratio, the ratio changes slightly after each iteration, mainly due to slight variation in gas dilution/mixing, and system background noise/fringes. The uncertainty of ratio over the ten calibration procedures was $\pm 0.12\%$ ($1\sigma$) for this work. The absolute concentration of $CO_2$ ($C_{\mathrm{CO_2}}$) is determined by the NDIR sensor. Once this procedure is complete, there is no need to re-calibrate in the field using standard gases.

At the present time we apply the peak-to-peak voltage of the $2f$ signals to determine the absorption magnitudes, which limits the minimum detectable concentration of NO to the peak-to-peak spectral noise corresponding to $\sim$ 10-ppb. Least squares fitting of the absorption features for NO and $CO_2$ using a reference spectrum (as described in [6]) has been found to improve the minimum detection limit to near 2-ppb. However, the lack of a reference arm makes this technique prone to error with changing laser tuning characteristics over time, such that the line positions of NO and $CO_2$ change with respect the reference $H_2O$ line used to align the spectra before coverage. Future work is needed to develop methods of accurate line centering of absorption features near the detection limit without significantly increasing instrument costs and complexities by the addition of a wavelength reference arm in the optical beam path.

## 3 Results of field study using the breathmeter

The TDLAS instrument, referred to as the Breathmeter, was used to measure the breath of 799 individuals over a period of more than one year ranging between September 28th, 2004 and November 23, 2005. Out of the 799 individuals tested, 769 of the tests were considered valid (a 96% success rate) in that two or more breath samples were successfully analyzed. Of the non-valid tests, some were due to software errors, but the majority were due to the volunteers' inability to donate breath properly according the procedures outlined above. Measurement of e$CO_2$ using both the NDIR sensor and the signal from the mid-IR laser absorption spectrum allowed for easy identification of valid and non-valid breath sample measurements. Volunteers were recruited from asthma screening events, health fairs, elementary and middle schools, two medical clinics, and from various visitors to the laboratory. A breakdown of the sample population by race and age is given in Table 1. Nurses, respiratory therapists, or instrument technicians operated the TDLAS system, entered patient data into the database, and explained the procedures for providing breath samples to the volunteers. Each volunteer was asked to give information regarding age, height, weight, gender, ethnicity, race, smoking status, health status regarding a prior diagnosis of asthma and related symptoms, and if applicable, the use of prescribed asthma medications (i.e., inhaled corticosteroids, rescue inhalers, etc.). A non-identifiable subject number was assigned to each volunteer and used to store the breath analysis measurement and self-reported data. Statistical differences in means between groups (i.e., mean eNO values for females vs. males) were determined using a t-test

| number tested in each age range by race | total tested | Age range 5–10 | 11–20 | 21–30 | 31–40 | 41–50 | > 50 |
|---|---|---|---|---|---|---|---|
| Am Indian/Alaska Native | 54 | 4 | 5 | 10 | 14 | 12 | 9 |
| Asian | 29 | 1 | 2 | 12 | 8 | 3 | 3 |
| Black/African American | 87 | 6 | 13 | 25 | 25 | 10 | 8 |
| Hawaiian/other | 12 | 2 | 1 | 3 | 1 | 4 | 1 |
| unknown/other | 32 | 3 | 2 | 7 | 15 | 2 | 3 |
| white | 555 | 50 | 77 | 103 | 109 | 105 | 111 |
| total tested by age | 769 | 66 | 100 | 160 | 172 | 136 | 135 |
| percent tested by age | 100% | 8.6% | 13% | 20.8% | 22.4% | 17.7% | 17.6% |

**TABLE 1** Sample population by race and age

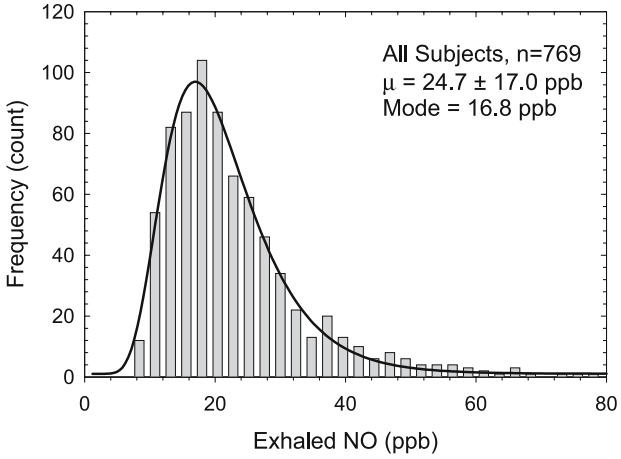


**FIGURE 5** Histogram of eNO concentrations for all subjects and the fitted log-normal curve ($r^2 = 0.98$)

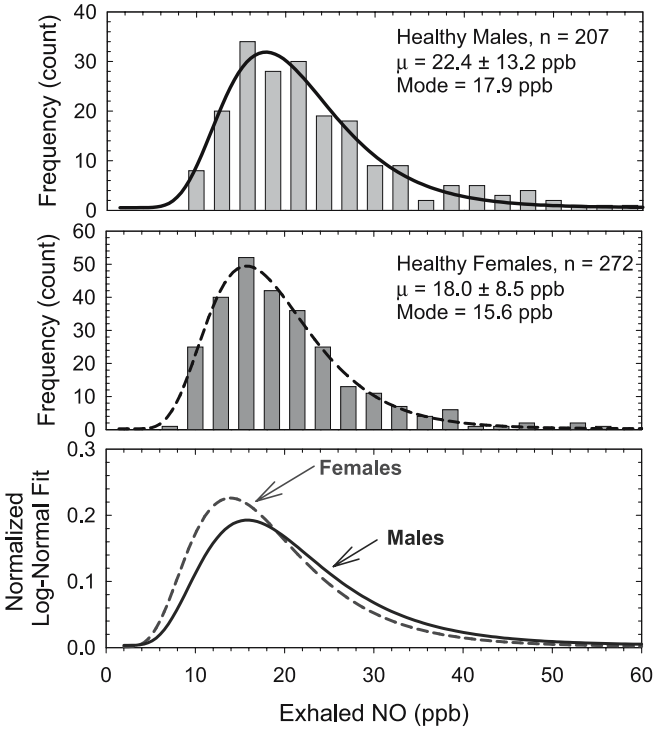


**FIGURE 6** (*Upper plot*) Histogram of measured eNO concentrations for healthy males and fitted log-normal curve, $r^2 = 0.96$. (*Middle plot*) Histogram of measured eNO concentrations for healthy females and fitted log-normal curve, $r^2 = 0.98$. (*Lower plot*) Fitted log-normal distribution curves for males (*solid blue line*) and females (*dashed red line*) for comparison

and p-values less than 0.05 were considered statistically significant.

Figure 5 shows a histogram of eNO levels measured from the 769 subjects who provided valid breath samples. The distribution of eNO follows a 4-parameter log-normal curve ($r^2 = 0.98$) with a mode centered at $\sim 16.8$ ppb and a mean and standard deviation of $24.7 \pm 17.0$ ppb. There was a significant and statistically meaningful difference in mean values (8.46 ppb) between those self-reporting a status of non-asthmatic ($19.9 \pm 10.98$ ppb, $n = 479$) versus a status of steroid naïve asthmatic ($28.36 \pm 22.95$ ppb, $n = 98$; $p < 0.001$). To note, steroid naïve patients with asthma are patients not taking any form of corticosteroid anti-inflammatory therapy, whether it be inhaled or orally administered. It is also interesting to note the statistical difference in mean eNO concentrations between healthy males and females ($22.42 \pm 13.19$ ppb, $n = 207$ and $18 \pm 8.49$ ppb, $n = 272$; $p < 0.001$), see histograms and log-normal fitted distributions in Fig. 6. Tsang and coworkers [17] and Wong and coworkers [18] both reported higher eNO concentrations in males as compared to females.

In our previous work [6, 7], $etCO_2$ concentration was assumed to be 4%, which leads to large errors in calculated eNO concentrations. Incorporating the NDIR sensor for direct independent measurement of $etCO_2$ concentrations has greatly improved the accuracy of determining eNO concentrations. Figure 7 shows a histogram of measured $etCO_2$ values for all subjects. The distribution follows a 3-parameter Gaussian curve ($r^2 = 0.96$) where the mean $etCO_2$ concentration was $4.55 \pm 0.65\%$ and ranged from approximately 3% to 7%. There was a statistically significant difference in mean $etCO_2$ levels between volunteers reporting a non-asthmatic and steroid naïve asthmatic status [$p < 0.05$; $4.62 \pm 0.69\%$, $n = 479$; and $4.47 \pm 0.65\%$, $n = 98$, respectively]. There was no significant difference in mean $etCO_2$ concentrations between healthy males and females [$p = 0.142$; $4.56 \pm 0.75\%$, $n = 207$ and $4.65 \pm 0.64\%$, $n = 272$].

Figure 8a and b show the inter-breath repeatability for NO and $CO_2$ for the three collected breath samples for all subjects tested, not excluding the individual breath tests that were considered to be outliers significantly differing from the other two tests. The replicate precision for NO was $1.7 \pm 1.89$ ppb with a mode at $\sim$ 1-ppb ($n = 769$). This represents excellent repeatability. The replicate precision for $CO_2$ was $0.28 \pm 0.22\%$ ($n = 769$). Both curves for NO and $CO_2$ replicate precisions follow a 5-parameter Weibull distribution ($r^2 = 0.98$ and $r^2 = 0.97$, respectively). The mean replicate precision for eNO is in good agreement with estimated precisions measured in the laboratory, where uncertainties encompass measurement uncertainties for the NO absorption line, the $CO_2$

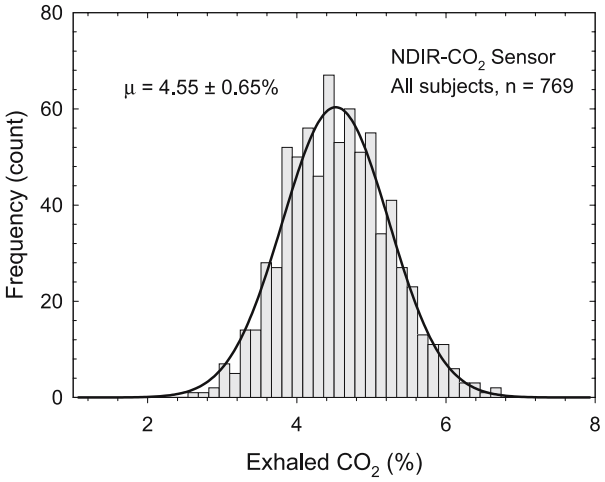


**FIGURE 7** (**a**) Histogram of $etCO_2$ values measured using the NDIR-$CO_2$ sensor for all subjects and fitted 3-parameter Gaussian curve, $r^2 = 0.96$. The mean exhaled $etCO_2$ was $4.55 \pm 0.65\%$

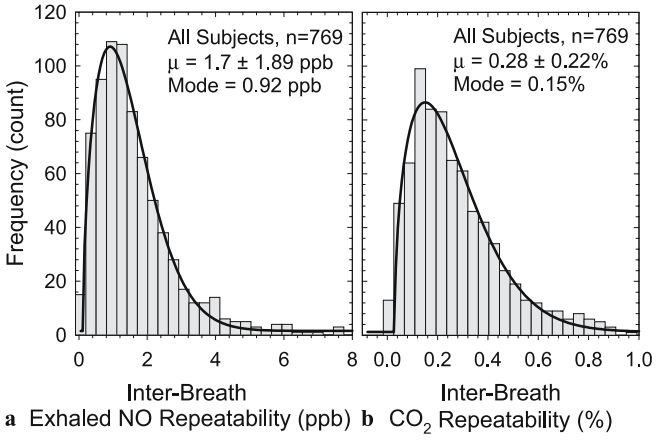


**FIGURE 8** Histograms of measured standard deviations from the results of each volunteer's three collected breath samples for (**a**) eNO, and (**b**) $etCO_2$ as measured with the NDIR-$CO_2$ sensor. Also plotted are the fitted Weibull curves to the histogram distributions with $r^2$ values of 0.97 and 0.98, respectively

absorption line, and absolute concentrations of $etCO_2$ made with the NDIR-$CO_2$ sensor. The total estimated error ($\sigma_{eNO}$), assuming normally distributed measurement noise, is given in (11) and is derived from (10):

$$C_{eNO} \pm \sigma_{eNO} = (k \pm \sigma_k) \frac{V_{NO} \pm \sigma_{V_{NO}}}{V_{CO_2} \pm \sigma_{V_{CO_2}}} \left[ C_{etCO_2} \pm \sigma_{etCO_2} \right], \tag{11}$$

where $\sigma_{V_{NO}}, \sigma_{V_{CO_2}}, \sigma_{etCO_2}$ represent the measurement precision error for the NO absorption line, the $CO_2$ absorption line, and the absolute concentration of $etCO_2$ as measured by the NDIR sensor, respectively, and $k$ is a constant that represents the slopes of the NO and $CO_2$ calibration curves in (10). To determine the measurement precision taking into account the uncertainty of the $etCO_2$ measurement, six measurements of 20-ppb NO and 5% $CO_2$ using standard gases were performed over a period of nine days. The TDLAS system measurement precision for calculated eNO using (11) was on average 2.06 ppb ($1\sigma$), and the accuracy over all days was $\pm 2.7$ ppb, assuming the true concentration of $CO_2$ was indeed 5%. Similarly, the $CO_2$ sensor was tested for accuracy and precision over the nine days and was found to be on the order of $\pm 0.23\%$ at an absolute $CO_2$ concentration of 5%. Computing the overall eNO uncertainty in quadrature gives a measurement precision uncertainty for eNO as defined in (11) of $\pm 2.8$ ppb ($1\sigma$) at 20-ppb and an uncertainty in the accuracy of $\pm 3.8$ ppb about the mean. However, precisions improve when multiple breath samples are taken and averaged, as is the case here. Commercial chemiluminescence instruments from Aerocrine report a measurement precision and accuracy of around $\pm 2.5$-ppb for absolute NO concentrations below 50-ppb. Future field studies using the Breathmeter will incorporate methods to analyze the long-term accuracy and precision of measurements using the ratio technique used here and will identify new spectral analysis algorithms to improve these metrics.

The effect of ambient NO (aNO) on measured eNO concentrations remains unclear as some reports have noted high aNO levels correlate to increased breath eNO concentrations, while others have not observed any correlation between aNO and measured eNO concentrations [19]. In the study presented here, volunteers did not inhale through a NO scrubber filter or inhale medical grade clean air devoid of NO. Figure 9 shows the log-normal fits of the eNO histogram from healthy individuals and the corresponding histogram for ambient NO concentrations. It should be noted that the mode for aNO of 11-ppb may more generally reflect the minimum detection limit of the sensor, but that values above this mode reflect true ambient NO levels. To examine the effects of aNO levels on measured mean eNO concentrations, healthy volunteers were sorted into two groups, one group tested when aNO concentrations were less than 20-ppb and the other group tested when aNO concentrations exceeded 20-ppb. Data where aNO levels could not be successfully quantified were removed, for example, if volunteers mistakenly began exhaling prior to the start of the test or the next sequential breath test started prior to the gas cell being completely flushed with ambient air. To account for mean differences found in males and females, each group was analyzed separately to determine the effects of aNO on measure eNO.

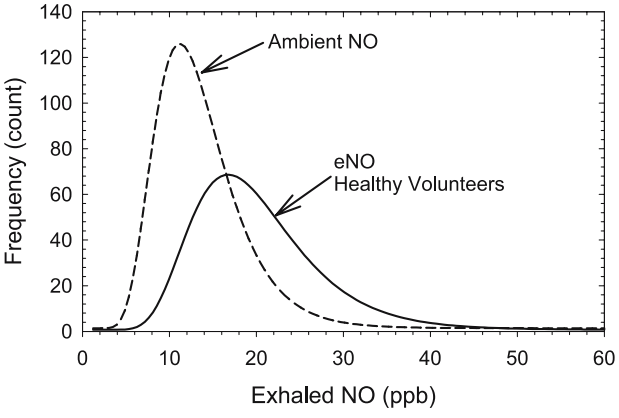


**FIGURE 9** Plot of the fitted 4-parameter log-normal curves for healthy volunteers ($r^2 = 0.98$) and respective measured ambient NO levels ($r^2 = 0.95$)

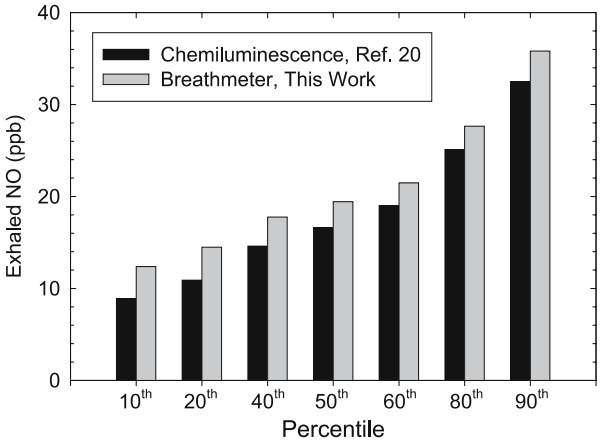


**FIGURE 10** Bar chart of measured percentiles from the 10th to the 90th of eNO from the study reported in [20] and the work reported here. Both populations consisted of healthy individuals not reporting any lung disease or symptoms

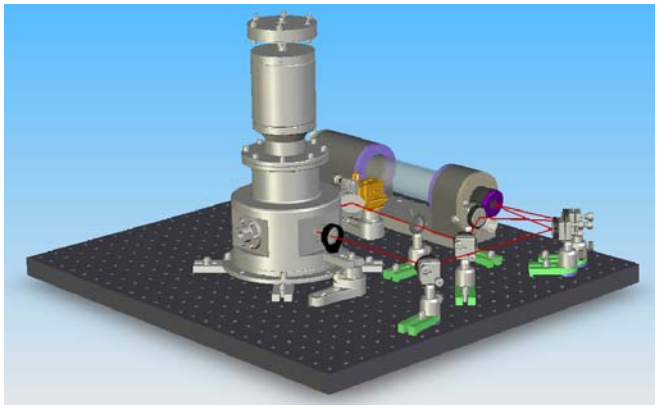

**FIGURE 11** A 3-D rendering of the next generation Breathmeter TDLAS system incorporating the use of a Stirling engine to provide cryogenic cooling for the laser and the detector in the vacuum tight housing. Also depicted are the various optics and 36-m Herriott cell. The red line represents the laser beam path. The length of the Herriott cell and the total height are both about 30 cm

Healthy females had a mean eNO concentration of $19.7 \pm 7.9$ ppb ($n = 196$) for aNO levels less than 20-ppb ($12.6 \pm 3.4$ ppb) and a mean eNO concentration of $21.1 \pm 7.8$ ($n = 40$) when aNO was > 20-ppb ($30.9 \pm 12.1$ ppb). Healthy males had a mean eNO concentration of $22.8 \pm 11.9$ ($n = 128$) with aNO < 20-ppb ($12.6 \pm 3.7$ ppb) and a mean eNO concentration of $24.4 \pm 10.3$ ppb ($n = 47$) with aNO > 20-ppb ($33.1 \pm 18.0$ ppb). Regardless of aNO concentration, there was no significant difference in mean eNO values for healthy females ($p = 0.31$) or healthy males ($p = 0.21$).

Examination of published literature suggests a close agreement in measured eNO levels in the healthy population reported here and reported elsewhere. Olin and coworkers published results of eNO concentrations measured from 1187 randomly selected non-smoking volunteers without respiratory symptoms using a chemiluminescence analyzer (Aerocrine's NIOX®) with an exhalation flow rate of 50 mL/s [20]. Figure 10 shows a comparison of the 10th through the 90th percentiles of the results obtained in this work using a TDLAS system (the Breathmeter) to the results published by Olin and coworkers [20]. A linear regression shows a strong correlation between the results ($r^2 = 0.99$), however, the Breathmeter measured, on average, an eNO concentration of $3.1 \pm 0.4$ ppb higher. A side-by-side instrument comparison using the same standard NO calibration gas would be required to determine if there exists any real differences in absolute measured eNO concentrations.

To reduce the size, weight, and the complexity of the TDLAS sensor presented here, the most current version of the instrument incorporates a Stirling engine in place of the closed-cycle cryogenic refrigerator unit. Figure 11 shows a 3-D rendering of the new optical platform including the 36-meter astigmatic Herriott cell, laser and detector housing with Stirling cooler, and assorted optical components described previously. The dimensions of the optical platform are 55 cm × 60 cm (length × width). Coupling the system with custom developed electronics for data acquisition, lock-in detection, spectral analysis, and laser control tailored for laser spectroscopic absorption spectroscopy will further improve performance and reduce cost and size.

## 4 Conclusion

Measurement of eNO concentrations in expired breath were performed across a diverse population of 769 volunteers, both children and adults. The TDLAS instrument operated without liquid nitrogen and without the need for routine calibration using standard gases. Precisions and accuracies determined in the laboratory were 2.8-ppb and 3.8-ppb ($1\sigma$), respectively. Analysis of collected breath data showed a mean replicate precision of $1.7 \pm 1.89$ ppb and a mode of 0.91 ppb. Measured eNO levels were log-normal and indicated a statistically significant difference in mean eNO concentrations between healthy males and females. Ambient NO levels did not significantly affect measured eNO levels, but further investigations regarding this issue are required. Additional collection and analysis of data to help understand the affects of age, height, weight and race on mean eNO levels are ongoing and will be published elsewhere.

**ACKNOWLEDGEMENTS** We gratefully acknowledge funding for this project from the Oklahoma Center for the Advancement of Science & Technology (contract number, AR02.1-051), the National Institutes of Health (contract number, 1R43HL70344-01), and the National Science Foundation (contract number, 0321447). We would also like to acknowledge Jason McCracken for his contributions in the analysis of NO and $CO_2$ distributions.

## REFERENCES

1 D.H. Yates, Immunol. Cell Biol. **79**, 178 (2001)
2 P.E. Silkoff, M. Carlson, T. Bourke, R. Katial, E. Ögren, S.J. Szefler, J. Allergy Clin. Immunol. **114**, 1242 (2004)
3 L.R. Narasimhan, W. Goodman, C.K.N. Patel, Proc. Nat. Acad. Sci. **98**, 4617 (2001)
4 K.D. Skeldon, M.G.M. Gibson, C.A. Wyse, L.C. McMillan, S.D. Monk, C. Longbottom, M.J. Padgett, Appl. Opt. **44**, 4712 (2005)
5 H. Dahnke, D. Kleine, P Hering, M. Mürtz, Appl. Phys. B **72**, 971 (2001)
6 C.B. Roller, K. Namjou, J. Jeffers, M. Camp, P.J. McCann, J. Grego, Appl. Opt. **41**, 6018 (2002)
7 C. Roller, K. Namjou, J. Jeffers, W. Potter, P.J. McCann, J. Grego, Opt. Lett. **27**, 107 (2002)
8 L. Menzel, A.A. Kosterev, F.K. Tittel, C. Gmachl, F. Capasso, D.L. Sivco, J.N. Baillargeon, A.L. Hutchinson, A.Y. Cho, W. Urban, Appl. Phys. B **72**, 859 (2001)

9 Y.A. Bakhirkin, A.A. Kosterev, R.F. Curl, F.K. Tittel, D.A. Yarekha, L. Hvozdara, M. Giovannini, J. Faist, Appl. Phys. B **82**, 149 (2006)
10 S.E. Ebeler, A.J. Clifford, T. Shibamoto, J. Chromatogr. B **702**, 211 (1997)
11 D. Smith, T. Wang, J. Sulé-Suso, P. Španěl, A.E. Haj, Rapid Commun. Mass Spectrom. **17**, 845 (2003)
12 S.M. Studer, J.B. Orens, I. Rosas, J.A. Krishnan, K.A. Cope, S. Yang, J.V. Conte, P.B. Becker, T.H. Risby, J. Heart Lung Transplant. **20**, 1158 (2001)
13 M. Phillips, M. Sabas, J. Greenberg, J. Clin. Pathol. **46**, 861 (1993)
14 B.S. Aldeen, D.M. Laskowski, R.A. Dweik, Proc. Am. Thoracic Soc. **3**, A310 (2006)
15 P.E. Silkoff, Am. J. Resp. Crit. Care **160**, 2104 (1999)
16 L.S. Rothman, C.P. Rinsland, A. Goldman, S.T. Massie, D.P. Edwards, J.M. Flaud, A. Perrin, C. Camy-Peret, V. Dana, J.Y. Mandin, J. Schroeder, A. McCann, R.R. Gamache, R.B. Wattson, K. Yoshino, K.V. Chance, K.W. Jucks, L.R. Brown, V. Nemtchinov, P. Varanasi, J. Quantum Spectrosc. Radiat. Transf. **60**, 665 (1998)
17 K.W. Tsang, S.K. Ip, R. Leung, G.L. Tipoe, S.L. Chan, I.H. Shum, M.S. Ip, C. Yan, P.C. Fung, M. Chan-Yeung, W. Lam, Lung **179**, 83 (2001)
18 G.W.K. Wong, E.K.H. Liu, T.F. Leung, E. Young, F.W.S. Ko, D.S.C. Hui, T.F. Fok, C.K.W. Lai, Clin. Exp. Allergy **35**, 889 (2005)
19 M. Bernareggi, G. Cremona, Pulmon. Pharmacol. Therap. **12**, 331 (1999)
20 A.-C. Olin, A. Rosengren, D. Thelle, K. Toren, Proc. Am. Thoracic Soc. **3**, A309 (2006)